PRELIMINARY WORK FOR DNS OF ROCKET-NOZZLE FILM-COOLING

J. M. F. Peter, M. J. Kloker
Institute of Aerodynamics and Gasdynamics, University of Stuttgart, Pfaffenwaldring 21, 70569 Stuttgart, Germany

Abstract

The supersonic flow in a conical nozzle with circular cross section is analyzed using RANS simulations to yield the boundary conditions for planned DNS of film cooling. A simplified one-species approach with calorically perfect gas assumption is used for the gaseous H_2O flow, and the results are compared to the experimental data of subproject A2, RWTH Aachen, of the collaborative research center SFB-TRR40. The influence of the wall temperature condition (adiabatic or isothermal with very low wall temperature) on the boundary layer at the cooling-slot position is investigated and the boundary-layer data at the cooling position are extracted. As a reference case the DNS of a fully turbulent boundary layer over a flat plate at Mach number 3.3 with zero pressure gradient and adiabatic wall is shown.

1. INTRODUCTION

The hot combustion gases of rocket motors lead to very high thermal loads on the engine walls, far exceeding the temperature limits of today's available materials, making active cooling indispensable. Next-generation rocket engines will have to withstand even higher heat loads due to an increase in combustion-chamber pressure and temperature for an increase in engine power. An effective method to protect the supersonic nozzle-extension flow is film cooling, where a cooling gas is blown into the hot-gas boundary-layer flow. This generates a protecting film that reduces the heat load into the structure at and downstream of the cooling-slot position by (i) a reduction of the wall temperature (in case of an adiabatic wall) or the temperature gradient (in case of an isothermal wall), and (ii) an alteration of the fluid properties such as heat capacity or conductivity (in case of foreign-gas injection). The cooling film can be generated either by wall-parallel blowing through a backward-facing step (see, e.g., [1–4]) or through wall-normal (or inclined) blowing through discrete holes or spanwise slits (see, e.g., [5–7]). Blowing through multiple, closely spaced holes or slits is generally referred to as effusion cooling, see, e.g., [8, 9]. Injecting the cooling gas through a porous wall is known as transpiration cooling, see, e.g., [10, 11]. The cooling effectiveness is governed by a complex interaction between the main and the coolant flow and depends on various parameters like cooling-gas type and temperature, mass flux, injection angle, or main flow characteristics. To investigate the flow behavior, numerical simulations are performed in this sub-project (SFB-TRR40-A4) to supplement the experimental investigations by sub-project A2. Previous numerical work in this sub-project was largely based on effusion cooling and a plane 2D nozzle experiment performed in A2, see, e.g., [12, 13] for the experimental and, e.g., [14, 15] for the numerical work. The experimental setup has now changed to a three-dimensional, axisymmetric nozzle with a circular cross section and conical contour. The film-cooling mechanism in this setup is planned to be analyzed in-depth using direct numerical simulations. To this end, the reference-case nozzle (no cooling) is analyzed using RANS simulations with the DLR TAU code to (i) get the boundary conditions for the DNS, and (ii) for general flow investigations to get an overview of the flow field. With the data obtained from the RANS simulations a DNS for a fully turbulent boundary layer is set up. As a first step, a zero-pressure-gradient flat-plate flow with adiabatic wall condition is considered. This will later be extended to include a backward-facing step with cooling gas injection, non-adiabatic walls and a pressure gradient.

This report is organized as follows: In Sec. 2 the film-cooling experiment will be briefly described. Section 3 provides the governing equations for the flow at hand. In Sec. 4 the numerical setup for the RANS and DNS simulations is explained in detail, and the simulation results are presented in Sec. 5. Finally, Sec. 6 summarizes the main findings and contains some concluding remarks.

2. FILM COOLING EXPERIMENT

In the experimental facility, rocket-engine-like stagnation conditions are achieved by means of a detonation tube. A hydrogen-oxygen mixture is burnt and the gases (superheated steam or gaseous H_2O, GH_2O) are brought to stagnation in a plenum chamber. This provides high pressures and temperatures for a short testing time in the order of 5-7 ms [16]. The axisymmetric nozzle is attached to the plenum chamber, and a vacuum tank on the exhaust side. For film-cooling experiments a circumferential injection slot is placed 84 mm downstream of the throat. The coolant is injected tangentially to the nozzle wall. Three different inserts for the slot geometry are available to vary the coolant exit Mach number; a fourth insert allows for a reference-case configuration without a cooling slot (plane nozzle wall). Static-pressure and heat-flux measurements are taken along an instrumented insert. Due to the short testing time the nozzle walls virtually remain at their initial temperature. To avoid condensation the walls have to be heated to at least 60° C. For more details on the experimental setup see [17]. The experimental configuration with a cooling-slot insert is depicted in Fig. 1 and the geometrical details of the nozzle are given in Tab. 1.

Length of expansion part, [mm]	340
Throat radius of curvature, [mm]	12
Throat diameter, [mm]	16
Convergent angle, [deg]	50
Divergent angle, [deg]	30
Expansion ratio, A_e/A^*	156
… at slot position, A_s/A^*	15

TAB 1. Geometric data of the axisymmetric nozzle.

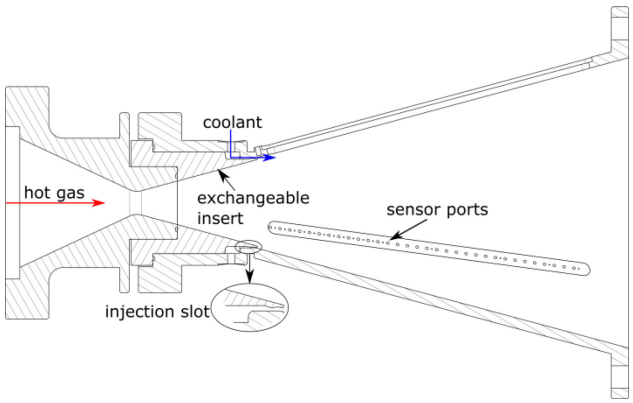

FIGURE 1. Experimental setup (here with cooling slot insert), taken from [17]

3. GOVERNING EQUATIONS

The governing equations for the flow of a gaseous fluid in a nozzle are the continuity equation, the three-dimensional compressible Navier-Stokes equations, the energy equation and an equation of state. Written in non-dimensional vectorized form, they can be found in, e.g., [24]. Sutherland's law can be used to calculate the dynamic viscosity μ as a function of temperature.

We do not consider the hydrogen/oxygen combustion in the detonation tube or any other chemical reaction throughout the nozzle. Instead, the main gas, i.e. superheated steam, is assumed to be a calorically perfect gas. For a calorically perfect gas the Prandtl number Pr and the ratio of specific heats $\kappa = c_p/c_v$ are assumed constant and the ideal gas law is used as equation of state. Due to the very high pressure and temperature in the plenum chamber this approach may not be fully appropriate. Also, the thermophysical gas properties are likely to vary over the nozzle due to the strong expansion. However, our focus is on the supersonic nozzle part where lower pressure and temperature prevail. Under the assumption of completely or at least partially frozen thermochemical kinetics after the nozzle throat, the calorically perfect gas approach may be reasonable. In fact, the results presented in Sec. 5 support this approach strongly. The thermophysical parameters for the hot GH_2O flow are listed in Tab. 2. Note that these values are the same (besides a slightly different value of $\kappa = 1.14$) as for a previous study of the plane 2D nozzle, see [18], where also a very good agreement with experimental data was achieved.

κ	1.15	Sutherland μ_{ref}	1.12e-5 [kg/(m*s)]
Pr	0.8	Sutherland C	1064 [K]
R_{H_2O}	461.5216 [J/kgK]	Sutherland T_{ref}	350 [K]

TAB 2. Thermophysical parameters of superheated steam.

4. NUMERICAL SETUP

Two different numerical tools are employed. For the full nozzle-flow calculations the TAU solver is used, which has been developed by the German Aerospace Center (DLR), and, for example, has been successfully applied to the numerical simulation of flows in dual-bell rocket nozzles [19]. For more details on TAU see, e.g., [20, 21]. For the corresponding direct numerical simulations of the turbulent boundary layer and the future film-cooling simulations the high-order in-house code NS3D is used. This code has been successfully used for the calculation of effusion cooling in supersonic boundary-layer flow [6, 22, 23]. Detailed information about NS3D can be found in, e.g., [7, 9, 23, 24]. All simulations are carried out on the CRAY XC40 Hazelhen supercomputer at the federal high performance computing center Stuttgart (HLRS).

4.1. Nozzle-flow calculations using DLR TAU

TAU uses a finite-volume approach for the spatial discretization of the governing equations. For this work we use the AUSMDV upwind flux-vector splitting scheme in combination with a least-square gradient reconstruction for a second-order discretization of the inviscid fluxes. The viscous fluxes are computed by a second-order central scheme. An explicit Runge-Kutta time-integration method is used for a stable initial start-up phase of the simulation and later switched to an implicit backward Euler method using the LU-SGS scheme for the solution of the linear equation system for faster convergence to steady state. A full multigrid scheme is used to accelerate the solution convergence. For the present work the Reynolds-averaged Navier-Stokes equations are solved applying different turbulence models. Note that no hydrogen/oxygen reaction mechanisms are considered in the current work, instead the main flow gas, i.e. superheated steam, is treated as a calorically perfect gas.
Computational grid, initial conditions, and boundary conditions: All simulations have been performed on two-dimensional axisymmetric hybrid structured/unstructured grids. The wall region is resolved with a finely structured grid. The wall-normal resolution is chosen such that $y^+ \leq 1$ holds above all viscous walls. For the interior nozzle region an unstructured grid is used. The simulations are initialized with an arbitrary subsonic flow in the whole domain. At the plenum inflow, a constant total pressure and total temperature condition is prescribed. The first part of the wall is assumed to belong to the plenum and is thus considered as adiabatic slip-wall. The wall of the converging part, the throat, and diverging part is a no-slip wall with either isothermal or adiabatic temperature condition. At the outflow, a simple

extrapolation is used to compute the flow values. The lower boundary is an axisymmetry axis. The setup for the nozzle-flow simulation is depicted in Fig. 2.

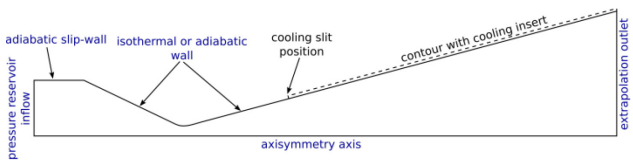

FIGURE 2. Setup for the TAU RANS simulations.

4.2. Direct numerical simulations using NS3D

NS3D is a high-order, block-structured, finite difference code for the time-accurate direct numerical simulation of compressible flows of one or two calorically perfect gases. (Alternatingly biased) compact finite differences of 6th-order are used for the spatial discretization in streamwise and wall-normal direction. To enable an independent solution of the resulting equation system for each computational domain for parallel computing, a sub-domain compact approach is used where the domain boundaries are coupled using explicit finite differences of 8th-order, see [22]. In the spanwise direction the flow is assumed periodic and a Fourier-spectral ansatz is used. The classical explicit 4th-order Runge-Kutta method is used for the time integration. In order to stabilize the computation a 10th-order compact filtering procedure can be applied to the conservative variables at a chosen time step interval. Strong gradients due to shocks can be treated by a shock-capturing procedure based on 2nd-order filtering [25].

Computational grid, initial conditions, and boundary conditions: The length scales for the DNS are non-dimensionalized by the boundary-layer thickness $\delta_{99,i}$ at the inlet. The regular domain extends from $34.4 \leq x/\delta_{99,i} \leq 217.7$ in the streamwise direction and has a height of $y/\delta_{99,i} = 20$. In the spanwise direction the domain has a width of approximately $14\ \delta_{99,i}$. In both wall-normal and streamwise direction an additional region with grid stretching is added to the regular domain to prevent numerical reflections at the boundaries. The origin of the coordinate system is placed on a virtual leading edge which is not part of the simulated domain. The simulation is initialized with a turbulent boundary-layer profile from a precursor simulation, which is scaled to yield the desired boundary-layer thickness at the inlet. At the wall, the no-slip, no-penetration boundary conditions are imposed on the velocity components. The pressure and temperature at the wall are extrapolated by a 5th-order polynomial according to $(\partial p/\partial y)_w = 0$ and $(\partial T/\partial y)_w = 0$, respectively (adiabatic wall condition); the density is calculated from the equation of state. At the freestream, a supersonic characteristic condition is used where all flow variables are computed such that the gradient along spatial characteristics is zero, except for the pressure, which is computed from the equation of state [26]. At the outflow, all flow quantities are extrapolated from the field using a 2nd-order parabola. At the supersonic inlet, all flow variables are fixed to the profile used as initial condition; additionally, unsteady artificial turbulent fluctuations using a digital filtering SEM method are superimposed within the boundary layer, see [27, 28]. Although the SEM method provides a pseudo-turbulent flowfield at the inlet of the domain, the flow needs about $10\ \delta_{99,i}$ in streamwise direction to fully satisfy equilibrium turbulent-flow statistics.

A sponge zone above the boundary layer in the inlet region prevents the farfield flow from being distorted by this transition process and also damps all shocks arising close to the inlet due to the supersonic condition. The computational setup is depicted in Fig. 3.

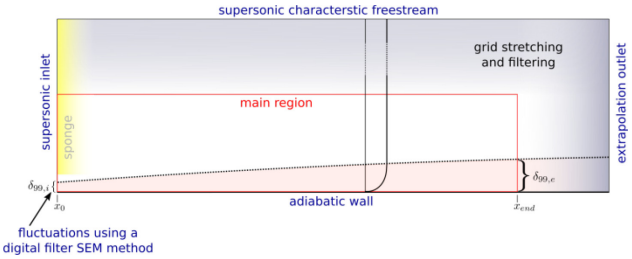

FIGURE 3. Setup for the boundary-layer DNS.

5. RESULTS

5.1. Nozzle flow

The plenum conditions for the nozzle flow simulations are chosen, according to the experiment, to be $p_0 = 30\ \mathrm{bar}$ and $T_0 = 3650\ \mathrm{K}$. The simulations have been run with either adiabatic or isothermal wall conditions, where the isothermal wall temperature is set, also according to the experiment, to $T_w = 333\ \mathrm{K}$. Three different turbulence models have been used, namely the one-equation Spalart-Allmaras model (SA), the two equation Wilcox k-ω model (k-ω), and the two-equation Menter-SST model (SST). Here, the Spalart-Allmaras model is defined as the reference case and is the model used unless otherwise noted. All simulations are considered fully turbulent. Note that due to the strong flow acceleration and wall cooling the flow may be also transitional. The thermophysical properties of the GH_2O flow are listed in Tab. 2. Note that these gas properties are consistent with values published in the literature, see, e.g. [29] or [30], but are tuned within their parameter range. The effects of a parameter variation for the gas properties are discussed below. Figure 4 shows the temperature distribution of the nozzle flow for the isothermal and adiabatic wall case. As expected, a large difference can be seen in the temperature gradient through the boundary layer between the two cases. The adiabatic wall temperature at the designated cooling slot position is $T_{w,ad} \approx 3500\ \mathrm{K}$, indicating the very strong wall-cooling effect present in the short-time experiment (throat: $T_{w,ad} \approx 3620\ \mathrm{K}$, exit: $T_{w,ad} \approx 3400\ \mathrm{K}$). Figure 5 shows the Mach number distribution in a close-up. Only minor differences exist between the two cases. A weak shock can be seen emanating from the transition point from the circular throat part to the conical diverging, straight part. This shock is reflected at the symmetry line and impacts the wall close to the designated cooling slot position. A possible influence of this shock on the cooling performance remains a subject of further investigations.

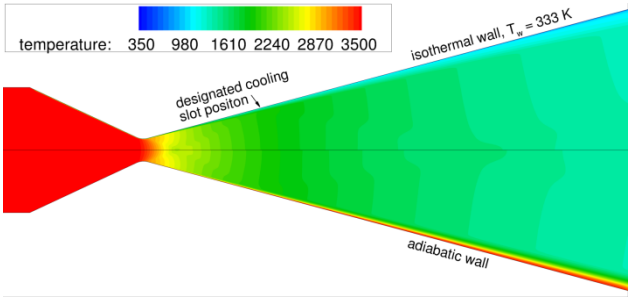

FIGURE 4. Temperature [K] contours for the nozzle flow, upper half: isothermal case, lower half: adabatic case.

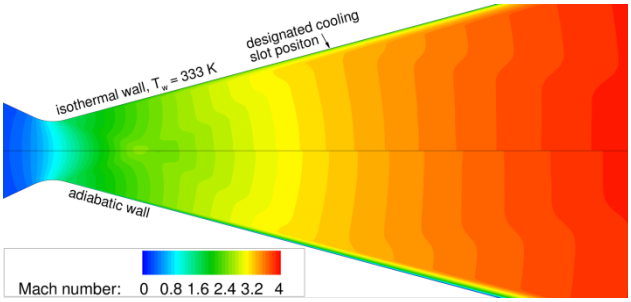

FIGURE 5. Mach number contours for the nozzle flow, upper half: isothermal case, lower half: adiabatic case.

Figure 6 compares the calculated heat flux and pressure distribution along the nozzle wall (isothermal case) with the experimentally measured data. A very good agreement can be obtained for the wall pressure. Some difference exists close to the exhaust region of the nozzle. This may be caused by the single-species approach or some measurement uncertainties, but a very good fit in the inner region, close to the designated cooling slot position at 84 mm, can be obtained. The numerically obtained heat flux also compares well with the experiment. The effect of the previously mentioned shock can also be seen in the curves. Additionally, the figure shows the results for two different ratios of specific heats, $\kappa = 1.17$, and $\kappa = 1.20$. The parameter has a large influence on both heat flux and pressure at the wall. While for $\kappa = 1.17$ the simulated heat flux compares even somewhat better to the experiment, the match for the pressure distribution gets worse, and for $\kappa = 1.20$ both curves compare less favorably to the experiment. A too low heat flux could theoretically be compensated by a reduction of the Prandtl number. While this increases the heat flux it has no effect on the wall pressure (not shown). The influence of the Sutherland values for viscosity has also been analyzed (not shown), but no influence on the wall pressure and only a negligible impact on the wall heat flux could be seen.

The main purpose of the nozzle flow simulation is to obtain the boundary conditions for the direct numerical simulation. Therefore, the flow at the designated cooling position is analyzed using the SA turbulence model, as well as the k- ω, and the SST model. The results are listed in Tab. 4 for the isothermal and the adiabatic case. For the freesteam values at the boundary-layer edge, such as Mach number or temperature, neither the wall condition nor the turbulence model shows a significant influence. In contrast, the thickness of the boundary layer δ_{99} depends on the wall temperature, with the adiabatic condition yielding a smaller value. Note that the effective shear-layer thickness is smaller with wall cooling, and the wall shear is higher. Quite some differences between the used turbulence models appear. The differences become even more evident for the integral values Re_θ and Re_τ. Here, not only the absolute values are much higher for the isothermal wall, but also the ratio is reversed compared to the adiabatic case.

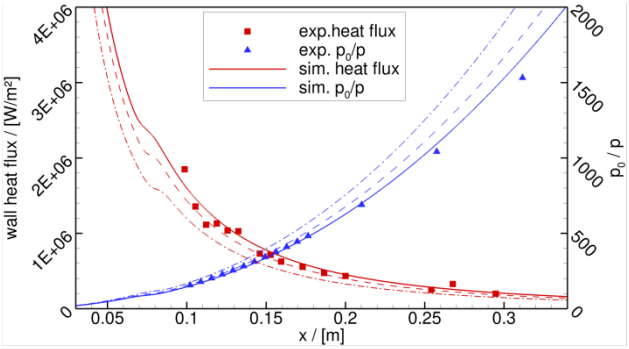

FIGURE 6. Comparison of simulated (isothermal case) and experimental heat flux [W/m²] and pressure ratio p_0/p distribution along the nozzle wall. Solid line: $\kappa = 1.15$, dashed line: $\kappa = 1.17$, dash-dotted line: $\kappa = 1.20$.

5.2. DNS of near-wall flow

To analyze the film-cooling mechanism in the nozzle using DNS the first step is a validated turbulent flow set-up for the given nozzle-flow conditions. Therefore, a direct numerical simulation for a fully turbulent flat-plate boundary layer using the NS3D code has been set-up. As a first reference case an adiabatic wall condition with zero pressure gradient is used. The simulation parameters are listed in Tab. 3, as taken from the previously discussed nozzle-flow results. The inflow boundary-layer thickness was chosen to be 3 mm. The fluid is again GH_2O, the thermophysical properties are listed in Tab. 2. The validation of a GH_2O flow proves difficult, due to the sparsity of different-from-air gas boundary-layer experiments or simulations available and the uncertainty of the influence of a different κ and Pr on turbulence statistics. Some important results will be shown below.

Ma_∞	3.3	[-]
T_∞	1980	[K]
p_∞	0.27963	[bar]
ρ_∞	0.0306	[kg/m³]
T_w	adiabatic	
$\delta_{99,i}$	3	[mm]

TAB 3. DNS simulation parameters.

The development of the skin-friction coefficient $c_f = \tau_w/(1/2\,\rho_w u_\infty^2)$ over Re_θ is shown in Fig. 7. The data from an incompressible DNS by Schlatter et al. [31] is shown together with a correlation curve $c_{f,inc} = 0.0024\,Re_\theta^{-0.25}$. Using the van Driest-II-transformation and the compressibility transformation suggested by Spalding and

Chi [32], a compressible correlation taking into account the ratio of specific heats κ and the Prandtl number Pr of GH_2O can be derived from the incompressible correlation [30]. The agreement between the present DNS and the correlation is very good. A small offset between the simulation result and the theoretical prediction exists. Note that the used incompressible correlation also under predicts the results from Schlatter for higher Re_θ. Two additional data points are shown for DNS of air at $Ma = 2.0$ [33] and at $Ma = 3.0$ [34] to illustrate the effect of a different main flow gas.

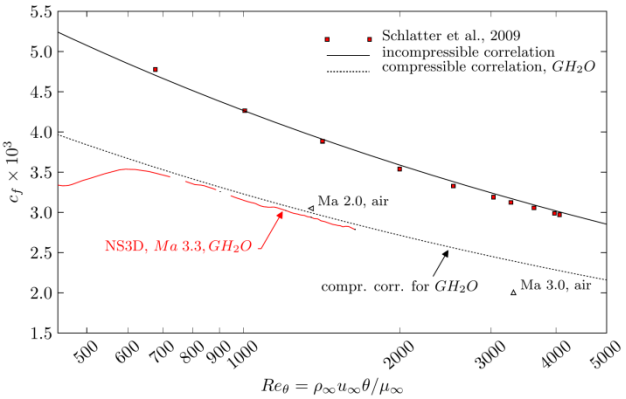

FIGURE 7. Comparison of skin friction coefficient c_f over Re_θ. Incompressible data from Schlatter et al. [31], for the derivation of the correlation curves see text.

The velocity fluctuations in inner scaling, e.g. $u^+_{rms} = \sqrt{u'u'}$, are shown in Fig. 8 and compared with data from a DNS of air at $Ma = 3.0$ from Pirozzoli [35]. Both results are plotted at $Re_\tau = 250$ and scaled according to Morkovin's hypothesis with the density ratio $\sqrt{\bar{\rho}/\rho_w}$ to account for compressibility. The agreement is very good throughout the boundary layer, although it remains unsure whether these statistics can be used for the validation of a non-air boundary layer. The pressure, temperature and density fluctuations (not shown) show no such quantitative comparability, but still a good qualitative agreement to other DNS of supersonic turbulent boundary layers (of air).

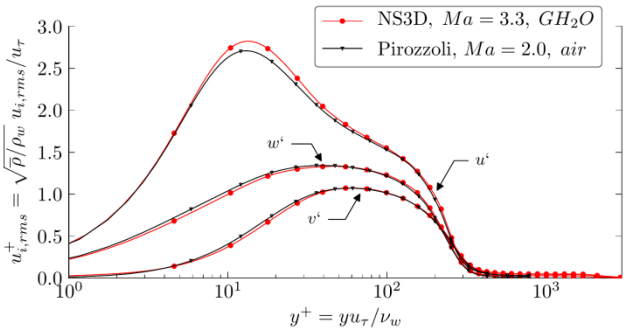

FIGURE 8. Comparison of density scaled rms velocity fluctuations u', v', w' in inner scaling between the DNS at hand and a $Ma = 2.0$ DNS of air from Pirozzoli [35], at $Re_\tau = 250$.

Snapshots of the u-velocity distribution in two wall-parallel planes are shown in Fig. 9. The inner region of the turbulent boundary layer is characterized by streamwise streaks, see the left plane at $y^+ = 5$, whereas the log-law region is dominated by larger structures, see the right plane at $y^+ = 50$. The near-wall streaks show a spacing of about 100 length units l^+ in inner scaling, which agrees well with the values for wall-bounded turbulent flows reported in the literature, see, e.g., [36]. Figure 10 shows a snapshot of the spanwise averaged density gradient to highlight the highly turbulent structure of the boundary layer as well as the large density gradient at the wall due to the adiabatic wall condition.

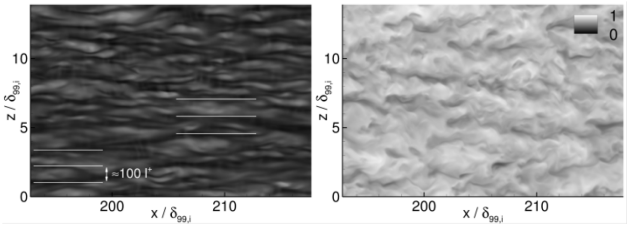

FIGURE 9. Snapshots of the u-velocity distribution at (left) $y^+ = 5$ and (right) $y^+ = 50$ from $Re_\theta = 1480\ to\ 1640$. The lines in the left figure are approx. 100 l^+ apart.

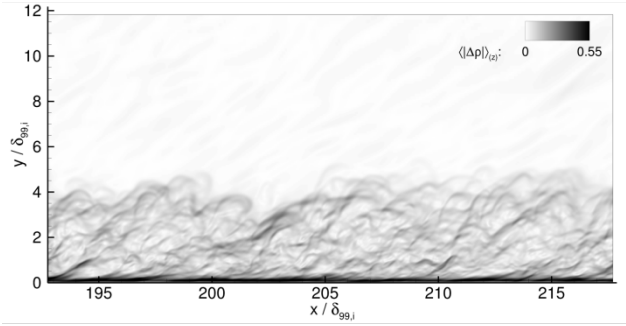

FIGURE 10. Snapshot of the spanwise averaged density gradient.

6. CONCLUSIONS

In preparation for the analysis of the film-cooling mechanism in supersonic rocket nozzles using direct numerical simulation, single-species RANS precursor simulations are performed to compute the flow field in a conical nozzle with circular cross section. These simulations serve as the basis for the planned film-cooling DNS. Note that we do not consider the hydrogen/oxygen combustion mechanism used in the experiment to generate the high stagnation pressures and temperatures. Instead, the flow is treated as a calorically perfect gas. This simplification yields very good agreement with the experimentally measured wall heat-flux and pressure distribution if κ and Pr are chosen appropriately. The wall temperature condition (adiabatic or isothermal with very low wall temperature) shows a very large influence on the boundary layer at the designated cooling-slot position, whereas the freestream values are much less affected. Also, a rather large influence of the employed turbulence model on the boundary layer can be seen. A fully turbulent flat-plate DNS of a GH_2O flow at a freestream Mach number of 3.3 with zero pressure gradient and adiabatic wall condition serves as a first reference case and is compared to other available data; the friction-coefficient evolution collapses with a compressible correlation formula. This simulation will serve as the basis for future film cooling investigations where details of the two-fluid flow field are scrutinized, especially the infection of the initially laminar cooling film with the cooling-film destroying

main-flow turbulence. In a next step, a backward-facing step will be implemented in the simulation and the blowing of the cooling gas into the turbulent main flow through the step will be analyzed.

	SA		k-ω		SST	
	isothermal	adiabatic	isothermal	adiabatic	isothermal	adiabatic
δ_{99} [mm]	2.5	2.2	3.7	2.7	2.7	2.3
Re_Θ	677	259	1040	302	839	265
Re_τ	1647	49	2843	62	2014	50
Ma_e	3.33	3.31	3.34	3.31	3.33	3.31
ρ_e [kg/m3]	0.0315	0.0327	0.0314	0.0328	0.0318	0.0328
T_e [K]	1983	2000	1967	2001	1985	2001

TAB 4. Boundary layer and boundary-layer edge data at the designated cooling slot position for different turbulence models for isothermal and adiabatic wall condition.

ACKNOWLEDGMENTS

Financial support has been provided by the German Research Foundation (Deutsche Forschungsgemeinschaft – DFG) in the framework of the Sonderforschungsbereich Transregio 40 (SFB-TRR40, SP A4). Computational resources have been provided by the High Performance Computing Center Stuttgart (HLRS) under project GCS_Lamt (LAMTUR).

[1] AUPOIX, B., MIGNOSI, A., VIALA, S., BOUVIER, F. and GAILLARD, R. (1998). Experimental and numerical study of supersonic film cooling. AIAA Journal, 36(6), 915–923.

[2] JUHANY, K.A. and HUNT, M.L. (1994). Flowfield measurement in supersonic film cooling including the effect of shock-wave interaction. AIAA Journal, 32(3), 578–585.

[3] KONOPKA, M., MEINKE, M. and SCHRÖDER, W. (2011). Large-eddy simulation of supersonic film cooling at finite pressure gradients. In: High Performance Computing in Science and Engineering. Springer Science + Business Media. 353–369. DOI 10.1007/978-3-642-23869-7_26.

[4] KELLER, M. and KLOKER, M.J. (2013). Wall-parallel cooling-gas injection in a laminar supersonic boundary-layer flow investigated by DNS. Tech. Rep. SFBTR40-2013, IAG-USTUTT. DOI 10.13140/RG.2.1.3548.1448.

[5] LINN, J. and KLOKER, M.J.(2008). Direct numerical simulation of film cooling in hypersonic boundary-layer flow. In: Nagel, W.E., Kröner, D.B. and Resch, M.M. (Eds.), High Performance Computing in Science and Engineering. Springer-Verlag.

[6] KELLER, M. and KLOKER, M.J. (2011). Influence of a favorable streamwise pressure gradient on laminar film cooling at Mach 2.67. In: 4th European Conference for Aerospace Science.

[7] KELLER, M. and KLOKER, M.J. (2016). Direct numerical simulation of foreign gas film cooling in supersonic boundary-layer flow. AIAA Journal, 55(1), 99–111. DOI http://dx.doi.org/10.2514/1.J055115.

[8] LINN, J. and KLOKER, M.J. (2011). Effects of wall-temperature conditions on effusion cooling in a supersonic boundary layer. AIAA Journal, 49(2), 299–307. DOI 10.2514/1.J050383.

[9] KELLER, M. and KLOKER, M.J. (2015). Effusion cooling and flow tripping and in laminar and supersonic boundary-layer and flow. AIAA Journal, 53(4). DOI 10.2514/1.J053251.

[10] [GÜLHAN, A. and BRAUN, S. (2011). An experimental study on the efficiency of transpiration cooling in laminar and turbulent hypersonic flows. Experimental Fluids, 50. DOI 10.1007/s00348-010-0945-6.

[11] LANGENER, T., and WOLFERSDORF, J. and STEELANT, J. (2011). Experimental investigations on transpiration cooling for scramjet applications using different coolants. AIAA Journal, 49(7). DOI 10.2514/1.J050698.

[12] YAHIAOUI, G. and OLIVIER, H. (2014). Calibration of a short-duration rocket nozzle film-cooling facility. In: Sonderforschungsbereich/Transregio 40 – Annual Report.

[13] YAHIAOUI, G. and OLIVIER, H. (2015). Supersonic film cooling in a high-enthalpy accelerated turbulent nozzle flow. In: Sonderforschungsbereich/Transregio 40 – Annual Report.

[14] KELLER, M. and KLOKER, M.J. (2014). Influence of Cooling-Gas Properties on Film-Cooling Effectiveness

in Supersonic Flow. Tech. Rep. SFB-TR40-2014, IAGUSTUTT. DOI 10.131140/RG.2.1.1450.9927.
[15] KELLER, M. and KLOKER, M.J. (2015). Foreign-Gas Film Cooling in Supersonic Turbulent Boundary-Layer Flow. Tech. Rep. SFB-TR40-2015, IAG-USTUTT. DOI 10.131140/RG.2.1.2761.7121/1.
[16] YAHIAOUI, G., HOMBSCH, M. and OLIVIER, H. (2013). Film cooling in a supersonic nozzle and a new high enthapy facility development. In: Sonderforschungsbereich/Transregio 40 – Annual Report.
[17] HAASE, S. and OLIVIER, H. (2016). Validation of an axisymmetric nozzle flow for film cooling experiments. In: Sonderforschungsbereich/Transregio 40 – Annual Report.
[18] KELLER, M. and KLOKER, M.J. (2016). Film cooling in Planar Nozzle Flows with Various Opening Angles. Tech. Rep. SFB-TR40-2016, IAG-USTUTT. DOI 10.131140/RG.2.2.12085.78564.
[19] SCHNEIDER, D., GÉNIN, C. and STARK, R. (2013). Numerical simulation of cold flow dual bell nozzles. In: Sonderforschungsbereich/Transregio 40 – Annual Report.
[20] MACK, A. and HANNEMANN, V. (2012). Validation of the unstructured DLR-TAU code for hypersonic flows. In: 32nd AIAA Fluid Dynamics Conference and Exhibit. DOI 10.2514/6.2002-3111.
[21] SCHWAMBORN, D., GERHOLD, T. and HEINRICH, R. (2006). The DLR TAU code: Recent applications in research and industry. In: European Conference on Computational Fluid Dynamics.
[22] KELLER, M. and KLOKER, M.J. (2013). Direct numerical simulations of film cooling in a supersonic boundary-layer flow on massively-parallel supercomputers. In: Sustained Simulation Per-formance. Springer Science + Business Media. ISBN http://id.crossref.org/isbn/978-3-319-01439-5, 107–128. DOI 10.1007/978-3-319-01439-5_8.
[23] KELLER, M. (2016). Numerical Investigation of Gaseous Film and Effusion Cooling in Supersonic Boundary-Layer Flows. Ph.D. thesis, University of Stuttgart.
[24] BABUCKE, A. (2009). Direct Numerical Simulation of Noise-Generation Mechanisms in the Mixing Layer of a Jet. Ph.D. thesis, University of Stuttgart.
[25] BOGEY, C., DE CACQUERAY, N. and BAILLY, C. (2009). A shock-capturing methodology based on adaptative spatial filtering for high-order non-linear computations. Journal of Computational Physics, 228(5), 1447–1465. ISSN 0021-9991. DOI 10.1016/j.jcp.2008.10.042.
[26] HARRIS, P.J. and FASEL, H.F. (1996). Numerical investigation of unsteady plane wakes at supersonic speeds. In: AIAA 34th Aerospace Sciences Meeting and Exhibit. DOI 10.25146/6.1996-686.
[27] KLEIN, M., SADIKI, A. and JANICKA, J. (2003). A digital filter based generation of inflow data for spatially developing direct numerical or large eddy simulations. Journal of Computational Physics, 186(2), 652–665. ISSN 0021-9991. DOI 10.1016/s0021-9991(03)00090-1.
[28] TOUBER, E. (2010). Unsteadiness in Shock-Wave/Boundary-Layer Interactions. Ph.D. thesis, University of Southampton.
[29] BIRD, R.B., STEWART, W.E. and LIGHTFOOT, E.N. (1960). Transport Phenomena. John Wiley & Sons Inc.
[30] WHITE, F.M. (2006). Viscous Fluid Flow. 3rd edn. McGraw-Hill.
[31] SCHLATTER, P., ÖRLÜ, R., LI, Q., BRETHOUWER, G., FRANSSON, J.H.M., JOHANSSON, A.V., ALFREDSSON, P.H. and HENNINGSON, D.S. (2009). Turbulent boundary layers up to Re_Θ=2500 studied through simulation and experiment. Physics of Fluids, 21(5). ISSN 1089-7666. DOI 10.1063/1.3139294.
[32] SPALDING, D.B. and CHI, S.W. (1964). The drag of a compressible turbulent boundary layer on a smooth flat plate with and without heat transfer. Journal of Fluid Mechanics, 18(1), 117–143. DOI 10.1017/S0022112064000088.
[33] PIROZZOLI, S., BERNARDINI, M. and GRASSO, F. (2008). Characterization of coherent vortical structures in a supersonic turbulent boundary layer. Journal of Fluid Mechanics, 613(205–231). DOI doi:10.1017/S0022112008003005.
[34] BERNARDINI, M. and PIROZZOLI, S. (2011). Wall pressure fluctuations beneath supersonic turbulent boundary layers. Physics of Fluids, 23. DOI 10.1063/1.3622773.
[35] PIROZZOLI, S. and BERNARDINI, M. (2011). Turbulence in supersonic boundary layers at moderate reynolds number. Journal of Fluid Mechanics, 688, 120–168. DOI 10.1017/jfm.2011.368.
[36] SMITH, C.R. and METZLER, S.P. (1983). The characteristics of low-speed streaks in the near-wall region of a turbulent boundary layer. Journal of Fluid Mechanics, 129, 27–54. DOI 10.1017/S0022112083000634.